Energy transfer and luminescent properties of Eu3+, Tb3+, Eu3+-Yb3+and Tb3+-Yb3+ doped α-NaYF4 nanophosphors prepared by coprecipitation route

Z. Smara, Y. Cheroura, D. Boyer, A. Potdevin, A. Chafa, O. Ziane, Rachid Mahiou

Energy transfer and luminescent properties of Eu^{3+}, Tb^{3+}, Eu^{3+}-$Yb^{3+}$and Tb^{3+}-Yb^{3+} doped α-$NaYF_4$ nanophosphors prepared by coprecipitation route

Z. Smara[1, 2], Y. Cheroura [1,3], D. Boyer[1*], A. Potdevin[1], A. Chafa[2], O. Ziane[3], R. Mahiou[1,*]

[1]Université Clermont Auvergne, CNRS, SIGMA Clermont, Institut de Chimie de Clermont-Ferrand, F-63000 Clermont-Ferrand, France
[2]Laboratoire des Sciences Nucléaires et Interaction Rayonnement Matière, Faculté de Physique, USTHB, El-Alia Bab-Ezzouar, 16111 Alger, Algérie
[3]Laboratoire d'Electronique Quantique, Faculté de Physique, USTHB, El-Alia Bab-Ezzouar, 16111 Alger, Algérie

[*]Corresponding Authors: damien.boyer@sigma-clermont.fr, rachid.mahiou@uca.fr

Abstract

Cubic α-$NaYF_4$ nanometer-sized crystals doped with Eu^{3+}, Tb^{3+}, Yb^{3+}-Eu^{3+} or Yb^{3+}-Tb^{3+} were synthesized by an original coprecipitation route. The obtained nanoparticles exhibited primary particles showing cubic shape with sizes ranging between 35 and 65 nm. The singly- or co-doped nanophosphors exhibited strong red (Eu^{3+}) or green (Tb^{3+}) fluorescence upon ultraviolet (UV) or near infrared (NIR) excitation, which resulted respectively from down- or up-conversion processes occurring in their structure. Spectroscopic properties were investigated on the basis of emission spectra as well as luminescence decays. From the emission spectra of Eu^{3+} doped samples, the Ω_2 and Ω_4 Judd-Ofelt intensity parameters were calculated. The concentration quenching of the Eu^{3+} or Tb^{3+} ion emissions in singly-doped or Yb^{3+} co-doped α-$NaYF_4$ were ascribed to resonant cross-relaxations. The main derived interaction between the active ions was evidenced as an electric dipole-dipole one through fitting the decays curves with the Inokuti-Hirayama model. The critical distances and energy transfer microparameters for the transfer processes were given showing very short range interaction. The dependence of integral up-conversion intensity on the NIR energy of the beam power was measured. The results indicated a two-photon process based on a cooperative energy transfer.

Keywords: Nanophosphors, Fluorides, Luminescence, Down-Conversion, Up-Conversion, Judd-Ofelt Theory

1. Introduction

Due to their transparency in the ultraviolet-visible range and their low phonon energies, fluorides are efficient hosts for up-conversion (UC) and down-conversion (DC) luminescence of rare earth (RE) ions [1]. Many applications of fluorides doped with RE have been performed, such as optical communications [2], lasers [3], display devices [4], and so on [5]. One of the most emerging applications resides on the use of rare-earth doped fluorides exhibiting both down (DC) and up (UC) conversions as solution for improving the energy efficiency of crystalline silicon (c-Si) solar cells as they can be used as mismatch media between the incident sunlight spectrum and the c-Si semiconductor [6]. However, to be applied on a c-Si, the DC and UC converters should be coupled onto the front surfaces of the cells [7]. Consequently, nanoparticles (NPs) with uniform distribution are required as host material, since they are expected to minimize scattering of incident sunlight [8].

Recently, rare-earth doped $NaYF_4$ nanocrystals were prepared with various methods like hydrothermal [9-11], solvothermal [12, 13], thermolysis [14], sol-gel [15], molten salt [16] and solid-state methods [17].

$NaYF_4$ nanocrystals may be prepared in two polymorphic forms, either cubic (α) or hexagonal (β) phases [18] depending on the synthesis conditions. The crystal structure of sodium yttrium fluoride has been the subject of debate for a long time. To obtain the cubic phase α-$NaYF_4$, several hydrothermal and solvothermal processes were utilized. Z. Wang *et al.* [9] used a hydrothermal route in a 30 mL autoclave, heated at 180°C for 24 h with the stoichiometry Y^{3+} : F^- = (1:4). G. Wang *et al.* [10, 12] used a 50 mL autoclave heated at 180°C for 24 h and a 30 mL autoclave heated at 160°C for 6 h. Y. Ma *et al.* [11] used a 50 mL autoclave heated at 180°C for 10 h. J. Wang *et al.* [13] synthesized this cubic form by a facile citric acid-assisted solvothermal process in a 100 mL Teflon-lined autoclave sealed and heated at 170°C for 12 h. But all these synthesis processes are energy consuming due to the high pressure conditions they imply, thus new energy efficient routes for preparing these fluorides as nanocrystals are requested. An alternative will consist in implementing a coprecipitation method to prepare $NaYF_4$ at low temperature and atmospheric pressure. Such a synthesis process was already used to obtain α-$NaYF_4$ but either as monodisperse microspheres [19] or as polydisperse nanoparticles [20].

In this work, we were able to synthesize nanoparticles of undoped and Eu^{3+}, Tb^{3+}, Eu^{3+}-$Yb^{3+}$and Tb^{3+}-Yb^{3+} doped cubic α-$NaYF_4$, *via* a facile approach at atmospheric pressure using a coprecipitation method on the basis of P. Lei *et al.* report [21] which is related to the preparation of β-$NaBiF_4$ nanocrystals. It was not possible to obtain the β hexagonal form in our case since the synthesis of this phase requires a temperature higher than 200°C [22], and the ethylene glycol (EG) used as the solvent in this procedure, has a boiling point of 180°C. Different temperatures and different reaction times were used to check the stability of the α-$NaYF_4$ matrices. The crystal structure and the morphology of the as-obtained NPs were assessed by XRD and TEM. Such analyses have allowed us to define accurately the parameters allowing to obtain pure α-$NaYF_4$ NPs with uniform size distribution. The defined procedure was used to prepare singly doped α-$NaYF_4$: Ln^{3+} and co-doped α-$NaYF_4$: Yb^{3+}, Ln^{3+} NPs (Ln^{3+}= Eu^{3+}, and Tb^{3+}). The choice of such ions is oriented by the fact they exhibit strong DC visible emissions under UV excitation, which fit nicely the absorption spectrum of

the c-Si cells. The activation by Yb^{3+} ions, which are well-known for their capability to efficiently absorb near IR radiations around ~ 1 μm and to convert them into the visible wavelength range by UC mechanism with codoping ions like Er^{3+}, Tm^{3+} or Ho^{3+} [23], was used to investigate such process in presence of both Eu^{3+} or Tb^{3+} for which only few reports exist [24].

Visible emissions from both singly doped and Yb^{3+} codoped α-$NaYF_4$ were analyzed through excitations in the UV and near IR as function of the Eu^{3+} or Tb^{3+} ions concentrations keeping the Yb^{3+} concentration fixed at 20 mol.%, value which generally corresponds to the upper limit for which no energy transfer between Yb^{3+} occurs, as reported in several papers [10-12]. In addition, the luminescence decays of the emitting levels were recorded and discussed in the frame of energy transfer mechanisms occurring between the active ions. As a result, we found that the site symmetry of the crystallographic sites on which the emitting ions are embedded in the NPs diverges and is lowered from the ideal cubic symmetry expected for cubic α-$NaYF_4$. For this reason, a Judd-Offelt calculation was done for a better understanding of the crystallographic properties and mechanisms of transitions in the case of Eu^{3+}.

2 - Experimental

2.1 - Materials and synthesis

Analytical grade yttrium nitrate hexahydrate ($Y(NO_3)_3.6H_2O$, 99.9 %), terbium nitrate pentahydrate ($Tb(NO_3)_3.5H_2O$, 99.9 %) and ytterbium nitrate pentahydrate ($Yb(NO_3)_3.5H_2O$, 99.9 %) were obtained from STREM CHEMICALS. Sodium nitrate ($NaNO_3$, 99.5 %) and ammonium fluoride (NH_4F, 95 %) were purchased from PROLAB. Ethylene glycol (EG) ($C_2H_2O_2$, 99.8 %) and europium nitrate pentahydrate ($Eu(NO_3)_3.5H_2O$, 99.9 %) were respectively purchased from ACROS ORGANICS and SIGMA-ALDRICH.

All the above chemicals materials were used directly without further purification.

The α-$NaYF_4$ nanoparticles were synthesized by a facile route, using the coprecipitation method as illustrated in Fig. 1. Firstly, solution 1 was prepared by dissolving 2 mmol of $NaNO_3$ and 1 mmol of $Y(NO_3)_3.6H_2O$ into 10 mL of EG. Meanwhile, the solution 2 was obtained by dissolving 6 mmol of NH_4F into 25 mL of EG under vigorous stirring. After that, the solution 1 was added gradually to the solution 2 under vigorous stirring. The resulting mixture was subsequently stirred at room temperature for different reaction times (30 min, 1 hour, 4 hours, 72 hours), and heated at different temperatures (30°C, 60°C, 100°C, 150°C) for 60 min. The final products were collected by centrifugation, washed several times with ethanol and water, and dried at 80 °C for one night.

Eu^{3+}, Tb^{3+}, Eu^{3+}-$Yb^{3+}$and Tb^{3+}-Yb^{3+} doped α-$NaYF_4$ were synthesized following the same procedure by using the optimal parameters of temperature and reaction time determined in the case of undoped α-$NaYF_4$.

2.2 – Characterization

The apparatus and the methods employed for identifying phases and analyzing their morphologies were already described previously [25].

The optical properties were investigated by recording the emission spectra with a Horiba-Jobin-Yvon set-up consisting of a Xenon lamp operating at 400 W monochromatized through Triax 180 then the emitted light was dispersed through Triax 550 and detected with the means

of a cryogenically cold charge coupled device (CCD) camera (Symphony LN2 series) for emission spectra.

Temporal evolution of the luminescence were carried out with a pulsed Nd:YAG OPO-Ekspla NT342B laser (3-5 ns pulse duration, 10 Hz, 5 cm^{-1} line width, 210-2600 nm). The emitted photons were detected at right angle from the excitation and analyzed through Edinburgh FLS980 spectrometer (1200 groove mm^{-1} grating, blazed at 500 nm, minimum band-pass of 0.1 nm) equipped with Hamamatsu R928P PMT (200-870 nm)

3- Results and discussion

3.1 - Structural and morphological analyses

Fig.2 reports the XRD patterns of undoped and doped α-$NaYF_4$ NPs prepared at room temperature for several times (30 min, 60 min, 1 hour, 4 hours, and 72 hours), and for 1 h at different temperatures (30°C, 60°C, 100°C, 150°C). The results indicate that, at room temperature (Fig. 2(a)), the reaction time has an influence on the crystallinity of the phases since, when the reaction time is longer than 30 min, the diffraction peaks are more intense. Depending on the temperature (Fig. 2(b)), the beginning of crystallization is observed for the sample obtained at 60 °C up to 150 °C for 1 hour of synthesis duration.

The XRD patterns of Eu^{3+} and Tb^{3+} doped α-$NaY_{(1-x)}F_4$ (x = 0.01, 0.05, 0.1, 0.2, 0.3) samples, and α-$NaYF_4$ doped 10 % Eu^{3+}or 10 % Tb^{3+}, codoped with 20 % Yb^{3+} are depicted in Fig. 2(c) and Fig. 2(d).

The XRD measurements indicate a relatively good crystallization of the samples, and all the diffraction peaks are well indexed using standard patterns of α-$NaYF_4$ *(space group Fm3m, JCPDS Card No. 01-077-2042).*

The calculated cell parameters are gathered in Tables S1 and S2 (Supporting information) for undoped α-$NaYF_4$ and singly doped α-$NaYF_4$ respectively with Eu^{3+} or Tb^{3+} ions.

To confirm the evolution of the crystalline cell as a function of the doping rate, the Vegard law has been drawn in the case of Eu^{3+} ion doping (Fig. S1). A linear increase in the cell volume is observed confirming the partial substitution of Y^{3+} ions ($r_{Y^{3+}}$ = 1.03Å for six-fold coordinated) by larger Eu^{3+} ions ($r_{Eu^{3+}}$ = 1.09Å for six-fold coordinated).

As observed at this stage, the crystallographic data indicate that the best conditions for obtaining pure crystallized phase of undoped α-$NaYF_4$ correspond to a synthesis at 60 °C for 1 hour. To confirm these most suitable parameters to achieve α-$NaYF_4$ NPs, transmission electron microscopy (TEM) analyses were carried out on the same samples. The pictures recorded from NPs synthesized at room temperature exhibit a cubic morphology whatever the synthesis time (Fig. S2). The edge length of nanocubes lies in the range of 37 to 50 nm depending on the synthesis duration. It is worth noticing that the mean particle size does not change too much between 4h and 72h since all the synthesis precursors have reacted.

Then by setting the synthesis time at 1h, several temperatures were investigated to prepare the α-$NaYF_4$ NPs. On the basis of the TEM pictures (Fig. 3), the most homogeneous and well-defined nanocubes were obtained at 60°C.

Thus, these conditions have been considered as the most optimized ones for synthesizing Eu^{3+}, Tb^{3+}, Yb^{3+}-Eu^{3+} and Yb^{3+}-Tb^{3+} doped α-$NaYF_4$ samples.

3.2 - IR spectroscopic studies

Fig. 4 gathers the ATR infrared spectra recorded in the range 4000-400 cm^{-1} from ethylene glycol, which was used as solvent, and α-$NaYF_4$:10 % Eu^{3+} as well as α-$NaYF_4$:10% Tb^{3+} synthesized at 60°C for 1 h. The interpretation of the spectra was made based on characteristic vibrational bands of EG [26, 27]. According to Table 1, the CH, OH, CC, and CO vibrations bands of EG are located in the region of 4000-500 cm^{-1}; so that they prove the existence of hydrophilic EG molecules coordinated onto the surface of fluorides nanocubes. This peculiar feature will have to be taken into account for further applications.

3.3 - Luminescence properties

All the measurements have been carried out at room temperature.

3.3.1 - Eu^{3+} doped and Eu^{3+}/Yb^{3+} co-doped α-$NaYF_4$

Fig. 5 shows the emission spectra of α-$NaYF_4$: Eu^{3+} (1, 5, 10, 20, 30 mol. %) nanocrystals, under 380 nm laser excitation. The emissions related to the $^5D_1 \rightarrow {}^7F_{0,\,1,\,2}$, and $^5D_0 \rightarrow {}^7F_{0,\,1,\,2,\,3,\,4}$ transitions of Eu^{3+} ions are observed. The $^5D_0 \rightarrow {}^7F_0$ transition is clearly observed on all the spectra. In addition, the intensity of the red $^5D_0 \rightarrow {}^7F_2$ emission is quite similar to that of the orange one ($^5D_0 \rightarrow {}^7F_1$). Such observations indicate that the local site symmetry of Eu^{3+} ions, which substitute one part of the Y^{3+} ions, is slightly lowered from the ideal cubic one, as commonly reported in the literature for Eu^{3+} doped α-$NaYF_4$.

The space group of α-$NaYF_4$ could be Fm3m, and Eu^{3+} ions substituting Y^{3+} ions would ideally possess a crystallographic site with point-group symmetry of O_h. The site occupation factors (SOF) and positional parameters of cubic $NaYF_4$ crystals are shown in Table 2.

The $^5D_0 \rightarrow {}^7F_{0,\,2,\,4}$ emissions should be strictly forbidden, because they are of forced electric-dipole, and only the magnetic-dipole transition of $^5D_0 \rightarrow {}^7F_1$ would be allowed [28].

According to the branching rules and transition selection rules of the 32 point groups [29], the highest site symmetry of Eu^{3+}, distorted from O_h, is C_s or C_2. The crystallographic site symmetry decreasing from O_h to C_s or C_2 was also observed in cubic $KLaF_4$ and $KGdF_4$ nanocrystals which exhibit the same crystal structure [28].

Fig. 6 reports the emission spectrum of α-$NaYF_4$ codoped with Eu^{3+} (10 mol. %) and Yb^{3+} (20 mol. %) under 973 nm excitation using OPO laser. We distinctly observe several bands centered at 590 nm, 613 nm, and 700 nm attributed to Eu^{3+} transitions. However, the emissions observed near 520, 540 and 650 nm correspond unambiguously to the $^2H_{11/2} \rightarrow {}^4I_{15/2}$, $^4S_{3/2} \rightarrow {}^4I_{15/2}$ and $^4F_{9/2} \rightarrow {}^4I_{15/2}$ transitions of Er^{3+} ions.

The parasitic emission peaks related to Er^{3+} in α-$NaYF_4$ are associated with the impurities existing in the Yb source (having up to 1500 ppm rare earth elements impurities according to the supplier). Such observation was already reported by T. K. Pathak *et al.* [30], which have analyzed the UC occurring in Eu^{3+}/Yb^{3+} co-doped α-$NaYF_4$ phosphor. Since the up-conversion connecting Yb^{3+} to Er^{3+} is an efficient process, these results prove that the up-conversion mechanism involving Yb^{3+} and Eu^{3+} ions has a weak efficacy but exists.

Fig. 7 reports the luminescence decays of the emissions arising from the $^5D_0$ level of Eu^{3+} under UV excitation at 380 nm. The shapes of the decays are independent of the monitored

$^5D_0 \rightarrow {}^7F_1$ or $^5D_0 \rightarrow {}^7F_2$ emission. For the low concentrations of Eu^{3+} ions, the decays exhibit a rise time which corresponds to the feeding of the $^5D_0$ level due to the de-excitation from the upper $^5D_1$ level. The time constant of this build-up in the case of α-$NaYF_4$:1%Eu^{3+} is around ~ 1 ms confirming that the non-radiative de-excitation connecting $^5D_1 \rightarrow {}^5D_0$ is weak. This rise is followed by an exponential decaying with a time constant around ~ 10-11 ms for the concentrations above 10 % content in Eu^{3+} ions. Beyond this concentration, the decays become non-exponential. The time constant measured in the tail of the decays spread from ~ 9.3 ms for the sample doped with 10 mol% Eu^{3+} to ~ 8 ms for the sample doped with 30 mol. % Eu^{3+}. These values are very high compared to that found in NPs of α-$NaYF_4$ doped with 1 mol. % Eu^{3+} prepared by emulsion-based wet chemical method, for which the reported lifetime for the $^5D_0$ level is of about 5.9 ms [31] but they are similar to that found in the bulk α-$NaYF_4$:0.5 % Eu^{3+} for which the measured lifetime of the $^5D_0$ level reached ~ 9 ms [32]. Since, in the case of NPs, several defects mainly at the surface of the NPs are known to reduce the radiative lifetime of active ions, such comparison clearly indicates that our samples are of very good quality. In the case of Eu^{3+}, the multiphonon relaxation rate is negligible as there is a large energy gap of about ~ 17300 cm^{-1} between the $^5D_0$ emitting level and the $^7F_0$ ground state (the transition $^5D_0 \rightarrow {}^7F_0$ lies at ~ 578 nm). Hence, lifetimes decrease by concentration quenching is mainly due to energy transfer through cross-relaxation. In the cross-relaxation process, an excited Eu^{3+} ion in the $^5D_0$ level is coupled with an unexcited one in its $^7F_0$ ground level by means of dipolar or multipolar interaction. Thus, such interaction promotes the unexcited Eu^{3+} ion in its first excited state of $^5D_0$ level. This process competes adversely with radiative relaxation and gives rise to the phenomenon of self-quenching fluorescence. Therefore, the energy transfer process between the Eu^{3+} activator ions provides an extra decay channel to change the decay curve profiles, resulting in a non-exponential decay curve.

The luminescence decays recorded with higher Eu^{3+} concentrations consist of an initial fast and non-exponential stage followed by a nearly exponential one, implying that the cross-relaxation rate is considerably higher than the rate of energy migration; accordingly, the experimental luminescence decay curves are expected to be consistent with theoretical time dependence predicted by the Inokuti-Hirayama (I-H) model [33, 34]:

$$I(t) = I_0 exp[-\frac{t}{\tau_0} - \frac{C_A}{C_0}\Gamma\left(1-\frac{3}{s}\right)\left(\frac{t}{\tau_0}\right)^{\frac{3}{s}}] \qquad (1)$$

where t = time; τ_0 = lifetime for low Eu^{3+} ion concentration; s = 6, 8, or 10 for dipole–dipole, dipole-quadrupole, or quadrupole-quadrupole interactions, respectively; and Γ(1-3/s) = 1.77, 1.43, and 1.30 for s = 6, 8, and 10 respectively. C_A is the concentration of acceptor ions. When the energy transfer process is the cross-relaxation within a system of identical ions, the acceptor concentration equals the total concentration of activators. C_0 is the critical concentration given by $C_0 = 3/(4\pi R_0^3)$ (R_0 is the critical transfer distance defined as the separation at which the rate of energy transfer between a donor-acceptor pair is equal to the intrinsic decay rate τ_0^{-1}). The donor-acceptor energy transfer parameter C_{DA} is related to R_0 as $C_{DA} = R_0^s x \tau_0^{-1}$.

When we set s = 6 [Γ(1-3/6) =1.77], τ_0 = 11 ms (being a lifetime value for Eu^{3+} dilute concentration sample like α-$NaY_{0.99}Eu_{0.01}F_4$), and treat C_A/C_0 as an adjustable parameter, the best fits of Eq. (1) (see details in Fig. 7; solid lines in Fig. 7 represent the best fit of Eq. (1)) to the experimental data are achieved, which leads us to conclude that the interaction between Eu^{3+} ions occurs *via* a dipole-dipole interaction. When the energy transfer process is the cross-relaxation within a system of identical ions, the acceptor concentration equals the total concentration of activators. The derived and calculated values are listed in Table 3.

The values of the critical radius R_0 are calculated for the decay curve of each sample and are consistent whatever the concentration (~ 3-4 Å). This value is short indicating that the interaction between two neighboring Eu^{3+} ions becomes efficient only for very large amount of activator ions.

Same procedure was used to analyze the luminescence decay of the $^5D_0$ excited state of Eu^{3+} in Yb^{3+}/Eu^{3+} co-doped α-$NaYF_4$ samples. The Eu^{3+} concentration was fixed at 10 % considering that this amount is the upper limit for which the interaction between two neighboring Eu^{3+} ions is weak. As observed on Fig. 8, the decay of the emission arising from the $^5D_0$ level diverges from a single exponential, notably at short times, in Yb^{3+}/Eu^{3+} co-doped α-$NaYF_4$ in comparison with the same decay recorded in the singly doped α-$NaYF_4$ with 10 mol. % in Eu^{3+}. This result is consistent with an energy transfer which occurs from the $^5D_0$ level of Eu^{3+} to Yb^{3+} neighbors. The results derived from the fitting by the I-H model are gathered in Table 4. Considering that both Eu^{3+} and Yb^{3+} act as acceptors or that only the Yb^{3+} ions are considered as acceptors, an R_0 value of ~ 4 and ~ 4.5 Å was obtained respectively.

These values are quite close each other indicating that the value used for C_A has a weak importance. However, the shape of the decay suggests that the $Eu^{3+} \rightarrow Yb^{3+}$ energy transfer occurs more probably at short time.

Fig. 9 reports the up-converted luminescence decays of the emissions peaking at 590 nm and 546 nm in Yb^{3+}/Eu^{3+} co-doped α-$NaYF_4$ under laser excitation at 973 nm. The decays present a rise time τ_R of respectively 0.2 ms and 8 μs followed by exponential decaying characterized by time constants τ_L of 3.3 ms and 103 μs respectively. These notable differences observed confirm that the emission located at 590 nm corresponds to the radiative de-excitation from the $^5D_0$ level of Eu^{3+} while the emission peaking at 546 nm corresponds to the de-excitation of the $^4S_{3/2}$ excited level of Er^{3+} ions present in the sample as impurities. In the case of Eu^{3+}, the value of τ_L is largely shorter than that of the radiative lifetime of the $^5D_0$ level under UV excitation (~ 9ms). Such observation indicates that perhaps energy “back transfer” can connect the Eu^{3+} ions to Yb^{3+} ions. Such consideration will be the subject of more convincing argument by recording the up-converted decays versus the Eu^{3+} concentration. At this stage, we can propose a schematic representation (Fig. 10) of the energy transfer mechanism that may occur in Yb^{3+}/Eu^{3+} co-doped α-$NaYF_4$ samples under NIR excitation into Yb^{3+} ions.

It is well-known that Eu^{3+} ions substitute Y^{3+} ions sites and this substitution almost does not affect the local environment. The intensity of the $^5D_0 \rightarrow {}^7F_2$ transition is extremely sensitive to chemical bonds in the vicinity of Eu^{3+}, and increases with the decrease in the site symmetry of Eu^{3+} center. On the other hand, the intensity of the $^5D_0 \rightarrow {}^7F_1$ transition is independent of the surroundings of Eu^{3+}. Therefore, the asymmetry ratio (R) is widely used as a criterion of the coordination state and the site symmetry for the RE ions. The higher the value of R is, the

lower the symmetry around the Eu^{3+} ions and the higher the Eu–O covalence are, and vice versa [35, 36].

The barycenters and the intensity ratios were determined and listed in Table 5 for α-$NaYF_4$: 1 % Eu^{3+}. Intensities of the main emission bands were normalized and compared to the standard reference $^5D_0 \rightarrow {}^7F_1$. Judd-Ofelt (J-O) [37, 38] intensity parameters are essential indicators in judging radiative potential of RE ions in different hosts, which are usually derived from absorption spectrum. Effective absorption measurement is very difficult for powdered phosphors. However, owing to the special energy level structure of Eu^{3+}, as stated above, they can be calculated from the emission spectra.

The asymmetry ratio R and J-O Ω_2 parameter reveal quite similar physical significance of the symmetric/asymmetric and covalent/ ionic bonding nature between Eu^{3+} ions and the surrounding ligands. Ω_2 is very sensitive to the environment in which Eu^{3+} ions exist. Therefore, the maximum value of Ω_2 can be related to changes in the structural environment around the Eu^{3+} ions because of the hypersensitivity of the $^5D_0 \rightarrow {}^7F_2$ transition. The larger Ω_2 parameter is a good indication that the symmetry of the Eu^{3+} sites is distorted [39, 40]. On the other hand, Ω_4 is related to the rigidity and stability of the matrix in which the rare earth ions are located [40, 41]. The J-O concepts and steps for the calculation of the Ω_t parameters have been reported in several papers and do not need to be repeated. For this reason, we shorten this presentation by retaining only two equations, since they are connected to the nature of the material [42].The transitions of Eu^{3+} from $^5D_0$ to ^7F_J (J=2–4) are electric dipole allowed and the spontaneous emission probability A from initial manifold J to terminal manifold J' is given using the following expression:

$$A(J;J') = \frac{64\pi^4\bar{\nu}^3}{3h(2J+1)}\left[\frac{n(n^2+2)^2}{9}\right]S_{ED} + n^3 S_{MD} \quad (2)$$

where n is the refractive index of the medium (n=1.432-1.438 [43]). υ is the average transition energy (in cm^{-1}), h is the Planck constant (6.63×10^{27} J.s) and (2J + 1) is the degeneracy of the initial state. S_{ED} and S_{MD} are the electric and magnetic dipole strengths. The strength of all induced dipole transitions can be calculated on basis of only three phenomenological J-O parameters using the following equation:

$$S_{ED}(5D_0; 7F_J) = e^2\Omega_t\left|\langle \Psi J|U^{(t)}|\Psi J'\rangle\right|^2 \quad (3)$$

where e is the elementary charge, and $\left|\langle \Psi J|U^{(t)}|\Psi J'\rangle\right|^2$ is the squared reduced matrix element of unit tensor operator which is independent of the chemical environment of the ion. For the case of Eu^{3+}, these values are given in ref. [44]. The derived values are reported in Table 6.

In Table 7, we have reported the calculated values of J-O $\Omega_{2,4}$ parameters.

The estimated value of radiative lifetime τ_R, for the $^5D_0$ level, derived from J-O theory using Eq.4 for α-$NaYF_4$: 1 % Eu^{3+} is around ~ 12.5 ms and close to that experimentally measured for this sample (~ 11 ms).

$$\frac{1}{\tau_R} = \sum_{j=1}^{j=4} A_{0j} \quad (4)$$

Only few works concern the cubic form α-$NaYF_4$:Eu^{3+}. The most important comparison deals with the value of 5.03 for Ω_2 parameter reported in the literature by P. Ghosh *et al.* [45]. Analyzing carefully this work, we found that the asymmetry ratio is close to that we have reported: around 1.3 in [46] 1.2 in [45] and 0.8 in our case. Since this ratio exhibits same information than the Ω_2 parameter, we suggest that our measurements are closer to the reality than the reported values in the literature, since these values diverge notably from the asymmetry ratio R measured on the depicted emission spectra under UV excitation: *ie* the $^5D_0 \rightarrow {}^7F_2$ electric dipole transition is forbidden in cubic symmetry leading to an asymmetric ratio R expected to be lower than 1. This is clearly illustrated in the Eu^{3+} doped α-$NaYF_4$ bulk for which R is 0.6 [32]. A possible explanation resides in the difference between the measured radiative lifetime of the $^5D_0$ level which is 9.35 ms in [46] and 5.6 ms in [45] while the value in our sample is 11 ms. Another possibility concerns the value of the refractive index. As reported in the case of nanocrystalline α-Lu_2O_3:Eu^{3+} [47], the radiative lifetime of an electronic transition of an ion embedded in a medium (air in our case) is correlated with an effective refractive index n_{eff}, which is a function of the intrinsic refractive index of the material and the fraction of space occupied by the NPs surrounded by the media with refractive index n_{med} [48]. The reported results [47] seem to indicate that both radiative lifetime and asymmetry ratio increase when the refractive index n_{med} decreases.
The obtained values for the branching ratios (Table 8) are very indicative and close to relative intensities between the main emission transitions connecting the first excited state $^5D_0$ to the manifolds ^7F_J (J = 0–4) as observed in Fig. 5.

3.3.2 - Tb^{3+} doped and Tb^{3+}/Yb^{3+} co-doped α-$NaYF_4$

The emission spectra of Tb^{3+} doped α-$NaYF_4$ samples upon excitation at 380 nm are gathered in Fig. 11 for several molar concentrations in Tb^{3+} ions. The emission bands centered at 489, 542, 588 and 620 nm correspond to the transitions connecting the first excited state $^5D_4$ of Tb^{3+} ion to ^7F_J manifolds of its ground state (J = 6, 5, 4, 3). The $^5D_4 \rightarrow {}^7F_5$ transition is the most intense as usually reported, conferring the characteristic green emission.
The transitions arising from the $^5D_3$ level are negligible compared to that issuing from the $^5D_4$ as observed in the inset of Fig. 11, indicating that the non-radiative de-excitation from the $^5D_3$ level is fast, probably by means of cross-relaxation mechanism, which is well established in the case of Tb^{3+} involving the quasi energy resonance between the $^5D_3 \rightarrow {}^7F_{0,1}$ emission and the $^7F_6 \rightarrow {}^5D_4$ absorption (Tb^{3+} ($^5D_3$) + Tb^{3+} ($^7F_6$) → Tb^{3+} ($^5D_4$) + Tb^{3+} ($^7F_{0,1}$)).
Same emission spectra are recorded for Tb^{3+}/Yb^{3+} co-doped α-$NaYF_4$ upon excitation at 380 nm (results not shown). Upon NIR excitation in the Yb^{3+} ion at 973 nm, only the emissions arising from the excited $^5D_4$ level are observed Fig. 12. A concentration of 10 % in Tb^{3+} ions was used in our experiments since the luminescence decay of the $^5D_4$ level of Tb^{3+} ions, under UV excitation, starts to diverge from single exponential from 20 % content in Tb^{3+} ions. 10% in Tb^{3+} was considered as the best concentration in our studies where no interaction between Tb^{3+} ions can occur allowing for a better understanding of the $Yb^{3+} \rightarrow Tb^{3+}$ mechanism.
Corresponding UC mechanism is proposed and illustrated in Fig. 13 in addition to the UV excitation. The incident photons at 973 nm are absorbed by the Yb^{3+} ions in the $^2F_{7/2}$ ground state and promoted in the $^2F_{5/2}$ excited state. Because the Tb^{3+} ions do not have corresponding energy levels in this range, after excitation of two Yb^{3+} ions, they can simultaneously transfer their energy to a Tb^{3+} ion lying in the $^7F_6$ ground state, which then is promoted to the excited $^5D_4$ level from which the luminescence occurs.

Fig. 14 shows decay curves of $^5D_4$ excited level of Tb^{3+} ions in α-$NaYF_4$: x % Tb^{3+} (x = 1, 5, 10, 20, and 30) under 380 nm excitation and monitoring the $^5D_4 \rightarrow {}^7F_5$ transition. A very short rise time (τ_R) is observed in the case of α-$NaYF_4$: 1 % Tb^{3+} confirming that the non-radiative de-excitation from the $^5D_3$ level is fast. The other decays are singly exponential with time constants of ~ 10-11 ms for the low concentrations. A shorter time constant of about 8 ms was recorded for 20 % Tb^{3+} content and the decays become non exponential for 30 % content in Tb^{3+} ions with a shorter time constant around 8 ms. As discussed above in the case of Eu^{3+} doped α-$NaYF_4$, we have considered that the non-exponential character of the decay is related to the interaction occurring between the active ions Tb^{3+}. For this reason, we have fitted this decay using I-H model. Considering that the intrinsic radiative lifetime of the $^5D_4$ level is ~11 ms, the parameters derived from the fit are gathered in Table 9.

The critical distance R_0 and energy transfer microparameter C_{DA} are the same than that obtained for Eu^{3+}. This observation is not surprising since the part of the exchange interaction is quite similar in the wave function of both $^5D_4$:Tb^{3+} and $^5D_0$:Eu^{3+} ions [49]. This means that the situation is not essentially different for Tb^{3+} than for Eu^{3+}, except that the $^5D_4$ and $^7F_6$ levels are connected by an optical transition with higher absorption strength than the $^7F_0$ and $^5D_0$ levels in the case of Eu^{3+}. The quenching of Tb^{3+} emission in singly doped α-$NaYF_4$ only reduces the luminescence lifetime by ≈50% in heavily (30 %) doped sample (estimation made by fitting the $^5D_4$ emission decay for this sample by bi-exponential function and using the time average determination as described in [50]). Same observation concerns the emission of Eu^{3+} in singly doped α-$NaYF_4$.

The decays of the $^5D_4$ level of Tb^{3+} in Tb^{3+}/Yb^{3+} co-doped α-$NaYF_4$ under UV excitation at 380 nm or NIR excitation at 973 nm are reported in Fig. 15. Under UV excitation the decay is exponential with a time constant of 7 ms. This value is lower than that found in singly doped 10 % Tb^{3+}: α-$NaYF_4$ for which the measured lifetime is about 9 ms. Such decrease is connected to the presence of Yb^{3+} ions indicating that a $Tb^{3+} \rightarrow Yb^{3+}$ energy transfer occurs. Under NIR excitation, the decay slightly diverges from single exponential, but remains relatively long with time constant in the tail of 6.5 ms which is close to that found in Tb^{3+}/Yb^{3+} doped α-$NaYF_4$ under UV excitation. Surprisingly, no rise time was recorded for this decay indicating that the UC mechanism is fast and the $Yb^{3+} \rightarrow Tb^{3+}$ energy transfer occurs mostly during the laser pulse. However, we have fitted this decay using I-H model. The derived parameters using τ_0 = 11 ms assuming that the concentration of ions acting as acceptor are only Tb^{3+} or Tb^{3+} in addition to Yb^{3+} are gathered in Table 10. Considering all the I-H fittings reported above, the critical distance R_0 remains always around 4 Å.

In order to determine the UC dynamics of Yb^{3+} / Tb^{3+} co-doped $NaYF_4$ nanocrystals, the power dependence of the UC luminescence have also been measured under NIR-CW excitation and shown in Fig. S3. The NIR power of the OPO laser did not allow checking the evolution of the luminescence decays versus the pump power. The photon processes involved can be achieved, according to the relation, $I \sim P^{(n)}$, where I is the measured UC intensity, P is the incident pump power, and n is the number of pump photons that are required for populating the upper emitting state [51]. The quadratic dependences illustrate that the green emission at 542 nm needs two-photon UC process. Same result was already reported for the

UC mechanism in Yb^{3+}/Tb^{3+}-codoped α-$NaYF_4$ nanocrystals synthesized by hydrothermal process [52].

Conclusion

In summary, α-$NaYF_4$ nanocubes, undoped, singly Eu^{3+} or Tb^{3+} doped as well as Eu^{3+}/Yb^{3+} and Tb^{3+}/Yb^{3+} co-doped were synthesized at 60°C during 1h by a facile route based on coprecipitation method in ethylene glycol. XRD analysis showed that all the products exhibit α-cubic $NaYF_4$ phase. The TEM images evidenced that the mean edge length of nanocubes (NCs) was 50 nm with small size dispersion. Under UV and NIR excitations, the luminescence spectra of singly doped samples showed the characteristics emission of Eu^{3+} or Tb^{3+} ions. Using the special character of Eu^{3+} as crystallographic local probe, we have discussed the Judd-Ofelt parameters calculated from the emission spectra of Eu^{3+} singly doped α-$NaYF_4$. The results indicate that the deformation of the crystallite sites is weak and the spectral distribution is close to that found in the bulk single crystal with pure cubic structure. Notably, the Ω_2 parameter derived from our measurement is not so far from the asymmetry ratio $R_{2\text{-}1}$ compared to the reported values in the literature for Eu^{3+} activated α-$NaYF_4$ nanoparticles. Decay curves of Eu^{3+} and Tb^{3+} in singly doped or Yb^{3+} co-doped NCs were analyzed under UV and NIR excitations. For both singly or co-doped samples, the decays are mainly exponential and diverge from the exponential when the concentration of active ions such as Eu^{3+} or Tb^{3+} is high or when the Yb^{3+} ion is added in the matrices. In that case, the decays are well fitted using Inokuti-Hirayama model for dipole-dipole interaction, for which the critical distance was found to be around 4~5 Å suggesting a dipolar interaction occurring at very short distance. Under NIR excitation, the kinetics decay time and pump power dependence analyses show that two Yb^{3+} ions can simultaneously transfer their energy to the first excited levels $^5D_0$ for Eu^{3+} and $^5D_4$ for Tb^{3+} from which two-photon emission occurs. The efficiency of such up-conversion process is acceptable in the case Yb^{3+}/Tb^{3+} pair while it is not in the case for Yb^{3+}/Eu^{3+} pair for which green and red luminescence are recorded because of the presence of Er^{3+} impurity.

Acknowledgements

This research was performed as a part of joint PHC, Tassili and Tassili Phase II, Algeria-France R&D Project (project N° 16MDU959) supported by Campus France (project N° 35079VB). Z.Smara and Y. Cheroura are grateful to the USTHB (Algeria) for providing a training grant under the faculty of physics program 2018-2019 and for the RI of UCA (France) for their facilities supports. We thank Christelle Blavignac (CICS, UCA) for TEM observations.

References

[1] G.J. De, W.P. Qin, J.S. Zhang, J.S. Zhang, Y. Wang, C.Y. Cao, Y. Cui, J. Infrared-to-ultraviolet up-conversion luminescence of YF_3 :Yb^{3+}, Tm^{3+} microsheets, J. Lumin. 122, (2007), 128–130, doi.org/10.1016/j.jlumin.2006.01.120

[2] P.M. Becker, A.A. Olsson, J.R. Simpson, Erbium-Doped Fiber Amplifiers: Fundamentals and Technology, Eds :Academic Press, San Diego, 1999, 460 pages, ASIN **:** B0089EM0NY

[3] R. Reisfeld, C.K. Jørgensen, Lasers and Excited States of Rare Earths, Springer, Berlin, 1977, 228 pages, ISBN-13 : 978-3-642-66698-8, doi.org/10.1007/978-3-642-66696-4

[4] G. Blasse, B.C. Grabmaier, Luminescent Materials, Springer, Verlag Berlin Heidelberg, 1994, 232 pages, ISBN 978-3-540-58019-5, doi.org/10.1007/978-3-642-79017-1

[5] F. Wang, D. Chatterjee, Z. Li, Y. Zhang, X. Fan, M. Wang, Synthesis of polyethylenimine / $NaYF_4$ nanoparticles with upconversion fluorescence, Nanotechnology, 17, (2006) 5786–5791, doi.org/10.1088/0957-4484/17/23/013

[6] B.S. Richards, Enhancing the performance of silicon solar cells via the application of passive luminescence conversion layers, Sol. Energy Mater. Sol. Cells. 90, (2006), 2329-2337, doi.org/10.1016/j.solmat.2006.03.035

[7] T. Trupke, M. A. Green, P. Würfel , Improving solar cell efficiencies by down-conversion of high-energy photons, J. Appl. Phys. 92, (2002), 1668-1674, doi.org/10.1063/1.1492021

[8] C. Lorbeer, J. Cybinska, A. Mudring, Facile preparation of quantum cutting GdF_3 : Eu^{3+} nanoparticles from ionic liquids, Chem. Commun. 46, (2010), 571-573, doi.org/10.1039/B919732J

[9] Z. Wang, F. Tao, L. Yao, W. Cai, X. Li, Selected synthesis of cubic and hexagonal $NaYF_4$ crystals via a complex-assisted hydrothermal route, J. Cryst. Growth. 290, (2006), 296–300, doi.org/10.1016/j.jcrysgro.2006.01.012

[10] G. Wang, W. Qin, L. Wang, G. Wei, P. Zhu, D. Zhang, F. Ding, Synthesis and upconversion luminescence properties of $NaYF_4$:Yb^{3+}/Er^{3+} microspheres, J. Rare Earths. 27, (2009), 394, doi.org/10.1016/S1002-0721(08)60258-6

[11] Y. Ma, M. Chen, M. Li, Hydrothermal synthesis of hydrophilic $NaYF_4$:Yb, Er nanoparticles with bright upconversion luminescence as biological label, Mater. Lett. 139, (2015), 22–25, doi.org/10.1016/j.matlet.2014.10.042

[12] G. Wang, W. Qin, J. Zhang, L. Wang, G. Wei, P. Zhu, R. Kim, Controlled synthesis and luminescence properties from cubic to hexagonal $NaYF_4$:Ln^{3+} (Ln = Eu and Yb/Tm) microcrystals, J. Alloy. Compd. 475, (2009), 452–455, doi.org/10.1016/j.jallcom.2008.07.050

[13] J. Wang, Y. Zhao, B. Li, L. Sun, J. Chen, Solvothermal synthesis and down / up conversion luminescence properties of Ln^{3+}-doped $NaYF_4$ nanocrystals, Mater. Lett. 93, (2013), 297–299, doi.org/10.1016/j.matlet.2012.11.094

[14] G. Chen, T. Y. Ohulchanskyy, R. Kumar, H. Agren, P. N. Prasad, Ultrasmall Monodisperse $NaYF_4$: Yb^{3+}/Tm^{3+} Nanocrystals with Enhanced Near-Infrared to Near-Infrared Upconversion Photoluminescence, ACS Nano, 4, (2010), 3163–3168, doi.org/10.1021/nn100457j

[15] X. Gao, N. Wang, T. Shi, S. Wang, M. Zhang, W. Zhang, J. Zhong, H. Tong, X. Zhang, Sol-gel synthesis of β-$NaYF_4$: $Yb^{3+}/Nd^{3+}/Tm^{3+}/Mn^{2+}$ nanophosphors and color-tunable upconversion luminescence, J. Fluorine Chem. 188, (2016), 23–27, doi.org/10.1016/j.jfluchem.2016.06.002

[16] X. Huang, G. Hu, Q. Xu, X. Li, Q. Yu, Molten-salt synthesis and up conversion of hexagonal $NaYF_4$: Er^{3+}:Yb^{3+} micro/nano-crystals, J. Alloys Comp. 616, (2014), 652–661, doi.org/10.1016/j.jallcom.2014.07.067

[17] A. A. Arnold, V. Terskikh, Q. Y. Li, R. Naccache, I. Marcotte, J. A. Capobianco, Structure of $NaYF_4$ Up converting Nanoparticles: A Multinuclear Solid-State NMR and DFT Computational Study, J. Phys. Chem. C. 117, (2013), 25733−25741, doi.org/10.1021/jp405813a

[18] J.F. Suyver, A. Aebischer, S. Garcia-Revilla, P. Gerner, H.U. Güdel, Anomalous power dependence of sensitized upconversion luminescence. Phys. Rev. B. 71, (2005), 125123, doi:10.1103/physrevb.71.125123

[19] Y. Han, S. Gai, P. Ma, L. Wang, M. Zhang, S. Huang, P. Yang, Highly Uniform α- $NaYF_4$:Yb/Er Hollow Microspheres and Their Application as Drug Carrier. Inorg. Chem. 52, (2013), 9184-9191, doi.org/10.1021/ic4001818

[20] N.O. Nunez, H. Miguez, M. Quintanilla, E. Cantelar, F. Cusso, M. Ocana, Synthesis of Spherical Down- and Up-Conversion $NaYF_4$-Based Nanophosphors with Tunable Size in Ethylene Glycol without Surfactants or Capping Additives. Eur. J. Inorg. Chem., (2008), 4517-4524, doi: 10.1002/ejic.200800363

[21] P. Lei, R. An, S. Yao, Q. Wang, L. Dong, X. Xu, K. Du, J. Feng, H. Zhang, Ultrafast Synthesis of Novel Hexagonal Phase $NaBiF_4$ Upconversion Nanoparticles at Room Temperature, Adv. Mater. 29, (2017), 1700505, doi.org/10.1002/adma.201700505

[22] H. Li, L. Xu, G. Chen , Controlled Synthesis of Monodisperse Hexagonal $NaYF_4$: Yb/Er Nanocrystals with Ultrasmall Size and Enhanced Upconversion Luminescence, Molecules, 22 (2017), 2113, doi.org/10.3390/molecules22122113

[23] N. Niu, F. He, S. Gai, C. Li, X. Zhang, S. Huang, P. Yang, Rapid microwave reflux process for the synthesis of pure hexagonal $NaYF_4$:Yb^{3+},Ln^{3+},Bi^{3+} (Ln^{3+} ¼ Er^{3+}, Tm^{3+}, Ho^{3+}) and its enhanced UC Luminescence, J. Mater. Chem. 22, (2012), 21613-21623, doi.org/10.1039/C2JM34653B

[24] K. Prorok, A. Gnach , A. Bednarkiewicz, W. Stręk. Energy up-conversion in Tb^{3+}/Yb^{3+} co-doped colloidal α-$NaYF_4$ nanocrystals, J. Lumin. 140, (2013), 103–109, doi.org/10.1016/j.jlumin.2013.03.012

[25] Y. Cheroura, Z. Smara, A. Potdevin, D. Boyer, A. Chafa, O. Ziane, R. Mahiou, Mater. Res. Bull. 125, (2020), 110809, doi.org/10.1016/j.materresbull.2020.110809]

[26] P. Buckley, P. A. Giguere, Infrared studies on rotational isomerism. I. Ethylene glycol, Can. J. Chem. 45, (1967), 397-407, doi.org/10.1139/v67-070

[27] G. Socrates, Infrared and Raman characteristic group frequencies tables and charts-Wiley (2001) Upconversion Photoluminescence, ACS Nano, 4, (2010), 3163–3168, doi.org/10.1021/nn100457j

[28] D. Tu, Y. Liu, H. Zhu, R. Li, L. Liu, U. Chen, Breakdown of Crystallographic Site Symmetry in Lanthanide-Doped $NaYF_4$, Angew. Chem. Int. Ed. 52, (2013), 1128 –1133, doi.org/10.1002/anie.201208218

[29] Q. Ju, Y. S. Liu, R. F. Li, L. Q. Liu, W. Q. Luo, X. Y. Chen, Optical Spectroscopy of Eu^{3+}-Doped BaFCl Nanocrystals, J. Phys. Chem. C. 113, (2009), 2309 – 2315, doi.org/10.1021/jp809233p

[30] T. K. Pathak, A. Kumar, L. J. Erasmus, A. Pandey, E. Coetsee, H. C. Swart, R. E. Kroon, Highly efficient infrared to visible up-conversion emission tuning fromred to white in Eu/Yb co-doped $NaYF_4$ phosphor, Spectrochim. Acta. A. 207, (2019), 23-30, doi.org/10.1016/j.saa.2018.08.064

[31] P. Ghosh, A. Patra, Tuning of Crystal Phase and Luminescence Properties of Eu^{3+} Doped Sodium Yttrium Fluoride Nanocrystals, J. Phys. Chem. C. 112, (2008), 3223-3231, doi.org/10.1021/jp7099114

[32] D. Jiang, H. Xia, J. Zhang, C. Wang, Z. Feng,S. He, Q. Tang, Q. Sheng, B. Chen & H. Jiang. Luminescent properties of Eu^{3+} doped α-$NaYF_4$ single crystal under NUV-excitation, J. Mod. Optic. 64, (2016), 164-169, doi.org/10.1080/09500340.2016.1218076

[33] M. Inokuti, F. Hirayama, Influence of Energy Transfer by the Exchange Mechanism on Donor Luminescence, J. Chem. Phys. 43, (1965), 1978-1989, doi.org/10.1063/1.1697063

[34] X. Zhang, W. Jiang, H. J. Seo, Analysis of Energy Transfer and Concentration Quenching in Sm^{3+}-Activated Borate Gd_3BO_6 Phosphors by Means of Fluorescence Dynamics, Spectrosc. Lett., 48, (2015), 27-31, doi.org/10.1080/00387010.20.2013.850778

[35] K. Binnemans, K. Van Herck, C. Görller-Walrand, Influence of dipicolinate ligands on the spectroscopic properties of europium (III) in solution, Chem. Phys. Lett. 266, (1997), 297–302, doi.org/10.1016/S0009-2614(97)00012-2

[36] R. Reisfeld, E. Zigansky, M. Gaft, Europium probe for estimation of site symmetry in glass films, glasses and crystals, Mol. Phys. 102, (2004), 1319–1330, doi.org/10.1080/00268970410001728609

[37] B.R. Judd, Optical absorption intensities of rare-earth ions, Phys. Rev. 127, (1962), 750–761, doi.org/10.1103/PhysRev.127.750

[38] G.S. Ofelt, Intensities of crystal spectra of rare-earth ions, J. Chem. Phys. 37, (1962), 511–520, doi.org/10.1063/1.1701366

[39] K. Binnemans, Interpretation of europium (III) spectra, Coord. Chem. Rev. 295, (2015), 1–45, doi.org/10.1016/j.ccr.2015.02.015

[40] C. Görller-Walrand, K. Binnemans, Spectral Intensities of Transitions, Handbook on the Physics and Chemistry of Rare Earths vol 25, Elsevier, 1998, 101–264, ISBN: 978-0-444-50185-1

[41] G. Anjaiah, S.K. Nayab Rasool, P. Kistaiah, Spectroscopic and visible luminescence properties of rare earth ions in lead fluoroborate glasses, J. Lumin. 159, (2015), 110–118, doi.org/10.1016/j.jlumin.2014.10.068

[42] S. Sebai, D. Zambon, A. Watras, P.J. Dereń, A. Megriche, R. Mahiou, Opt. Mater. 92, (2019), 217–222, https://doi.org/10.1016/j.optmat.2019.04.037]

[43] R. E. Thoma, G. M. Hebert, H. Insley, C. F. Weaver, Phase Equilibria in the System Sodium Fluoride-Yttrium Fluoride, Inorg. Chem. 2, (1963), 1005-1012.

[44] W.T. Carnall, H. Crosswhite, H.M. Crosswhite, Energy Level Structure and Transition Probabilities in the Spectra of the Trivalent Lanthanides in LaF_3, Report Argonne National Laboratory, Chemistry Division, Argonne IL, 1977

[45] P. Ghosh, A. Patra, Influence of Crystal Phase and Excitation Wavelength on Luminescence Properties of Eu^{3+}-Doped Sodium Yttrium Fluoride Nanocrystals, J. Phys. Chem. C. 112, (2008), 19283-19292, doi.org/10.1021/jp807539r

[46] C. Cao, H. K. Yang, J. W. Chung, B. K. Moon, B. C. Choi, J. H. Jeong, K. H. Kim, Hydrothermal synthesis and optical properties of Eu^{3+} doped $NaREF_4$ (RE = Y, Gd), LnF_3 (Ln = Y, La), and $YF_3 1.5NH_3$ micro/nanocrystals, Mater. Res. Bull. 46, (2011), 1553–1559, doi.org/10.1016/j.materresbull.2011.06.026

[47] J. C. Boyer, F. Vetrone, J. A. Capobianco, A. Speghini, and M. Bettinelli, Variation of Fluorescence Lifetimes and Judd-Ofelt Parameters between Eu^{3+} Doped Bulk and Nanocrystalline Cubic Lu_2O_3, J. Phys. Chem B. 108, (2004), 20137-20143, doi.org/10.1021/jp0480504

[48] R. Meltzer, S. P. Feofilov, B. Tissue, H. B. Yuan Dependence of fluorescence lifetimes of Y_2O_3:Eu^{3+} nanoparticles on the surrounding medium, Phys. Rev. B. 60, (1999), 14012-14015, doi.org/10.1103/PhysRevB.60.R14012

[49] G. Blasse, Luminescence of inorganic solids: from isolated centres to concentrated systems, Prog. Solid. St. Chem. 18, (1988), 79-171, doi.org/10.1016/0079-6786(88)90004-0

[50] R. K. Bauer, P. de Mayo, L.V. Natarajan, W. R. Ware, Can. Surface photochemistry: the effect of surface modification on the photophysics of naphthalene and pyrene adsorbed on silica gel, J. Chem. 62, (1984), 1279-1286, doi.org/10.1139/v84-213

[51] B. P. Sobolev, D. A. Mineev, V. P. Pashutin, Low temperature hexagonal modification of $NaYF_4$ having the gagarinite structure, Dokl. Akad. Nauk SSSR, 150, (1963), 791–794.

[52] H. Liang, G. Chen. Li. Liu, F. Qin, Z. Zhang, Upconversion luminescence in Yb^{3+}/Tb^{3+} codoped monodisperse $NaYF_4$ nanocrystals, Opt. Commun. 282, (2009), 3028-3031, doi.org/10.1016/j.optcom.2009.04.006

Fig. 1. Schematic diagram describing the synthesis process of α-$NaYF_4$ nanoparticles.

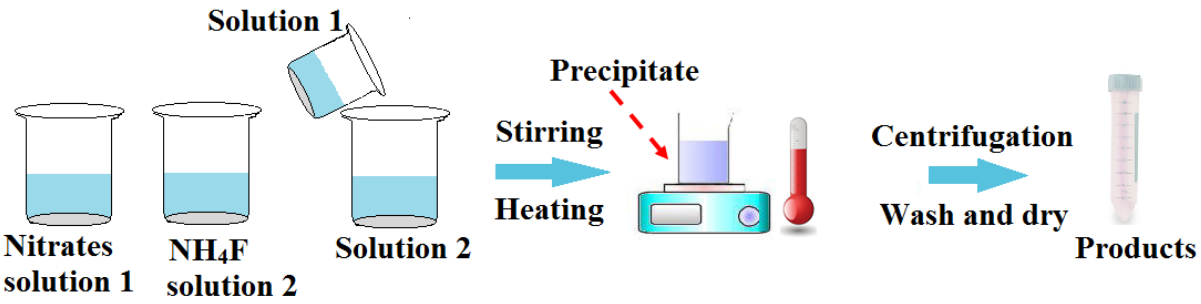

Fig. 2. XRD patterns of α-$NaYF_4$ NPs (a) synthesized at room temperature for different reaction time, (b) synthesized at 30°C, 60°C, 100°C, and 150°C for 1 hour, (c) XRD patterns of Tb^{3+} doped α-$NaYF_4$ NPs synthesized at 60°C for 1 h, and co-doped with 20 % Yb^{3+} / 10 % Tb^{3+} and (d) XRD patterns of Eu^{3+} doped α-$NaYF_4$ NPs synthesized at 60°C for 1 h, and co-doped with 20 % Yb^{3+} / 10 % Eu^{3+}.

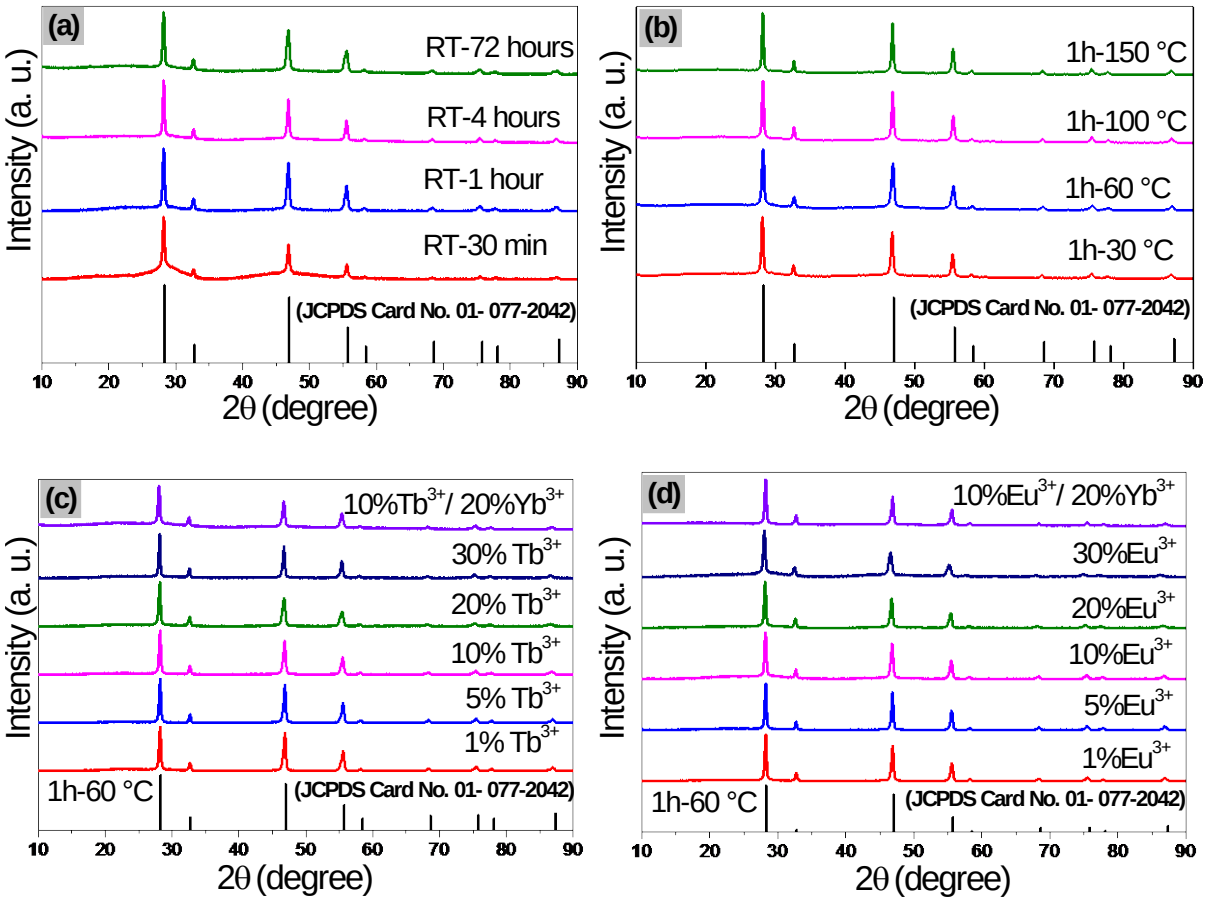

Fig. 3. TEM of α-$NaYF_4$ for one hour of reaction time at different temperatures: (a) 60°C, (b) 100°C, (c) 150°C and corresponding particles size distribution.

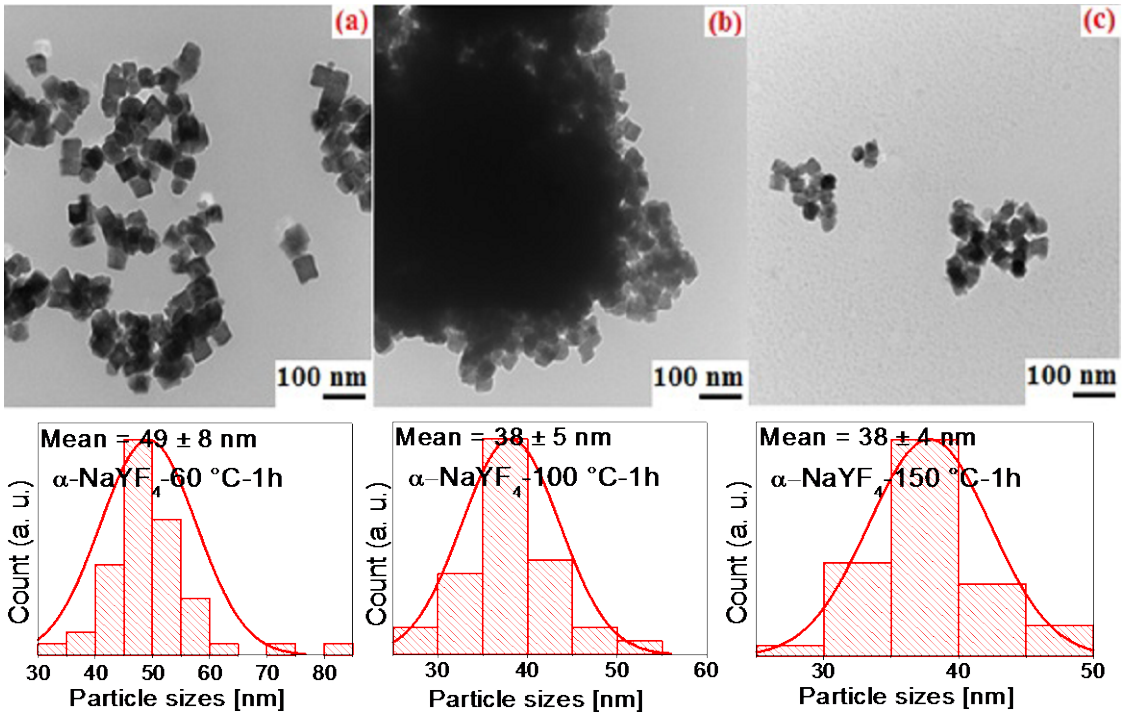

Fig. 4. Infrared spectra of EG, α-$NaYF_4$: 10 % Eu^{3+}, and α-$NaYF_4$: 10 % Tb^{3+} samples.

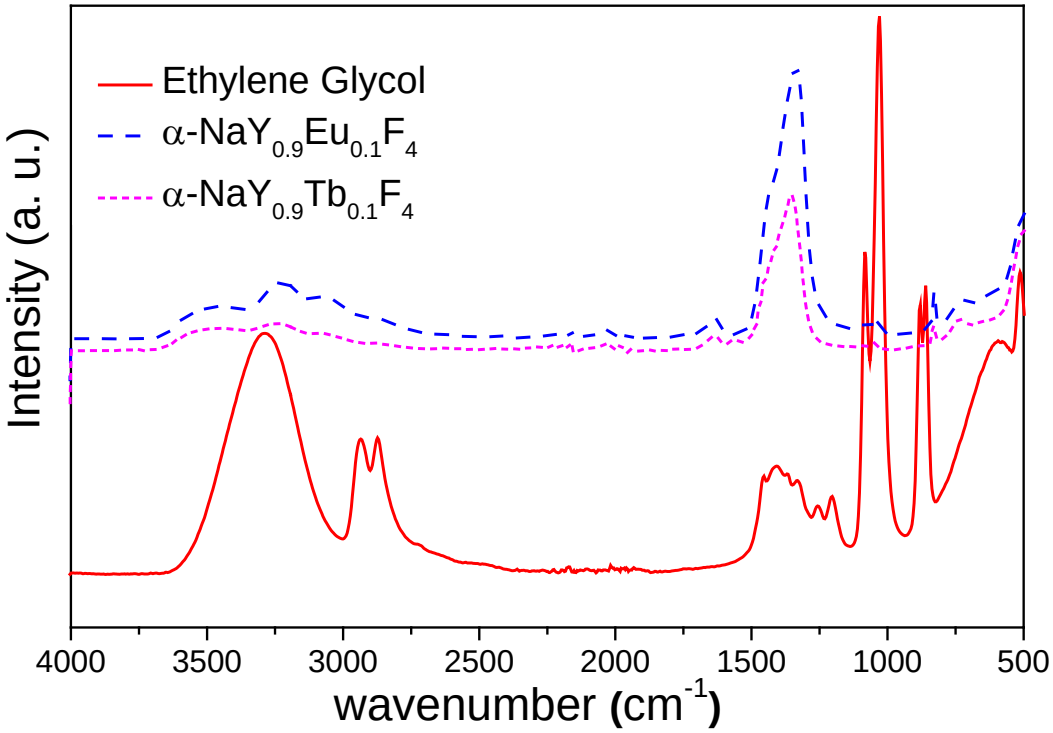

Fig. 5. Emission spectra of α-$NaYF_4$ doped (1, 5, 10, 20, 30) % Eu^{3+} under UV excitation at 380 nm.

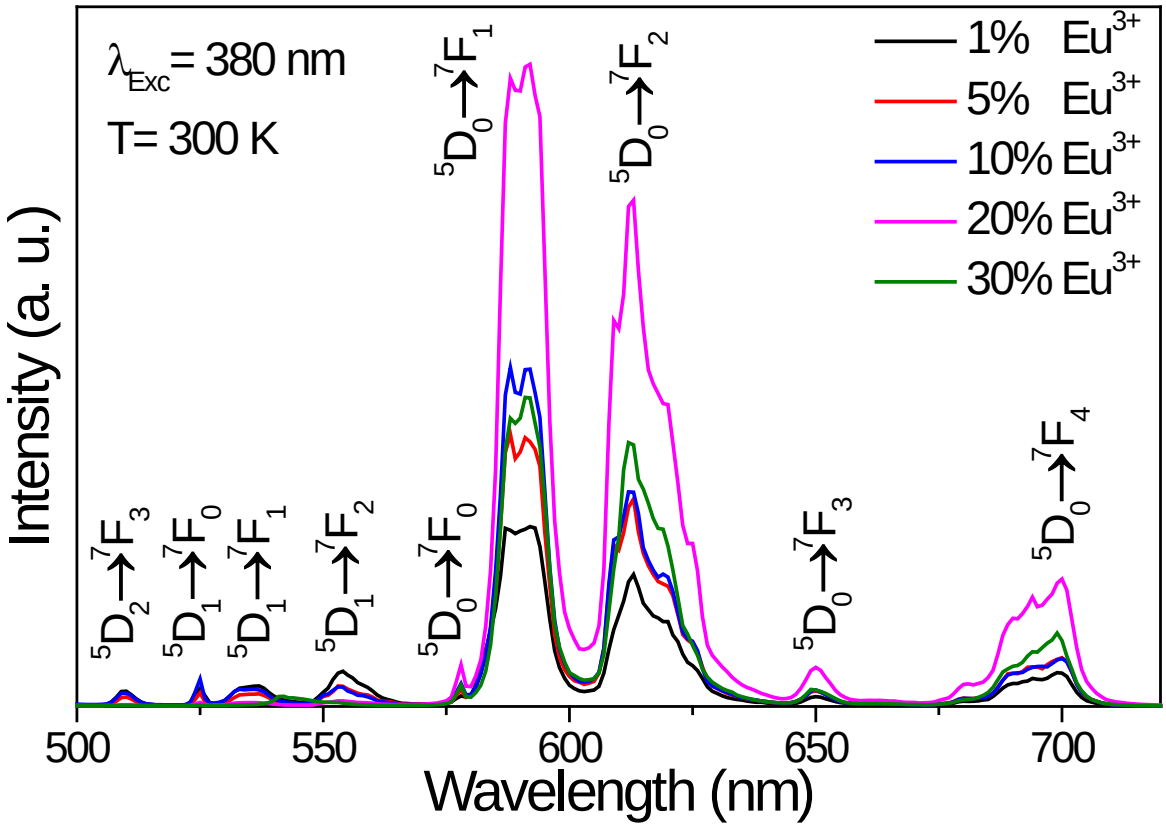

Fig. 6. Emission spectra of α-$NaYF_4$ co-doped 10% Eu^{3+} / 20 % Yb^{3+} under 973nm excitation.

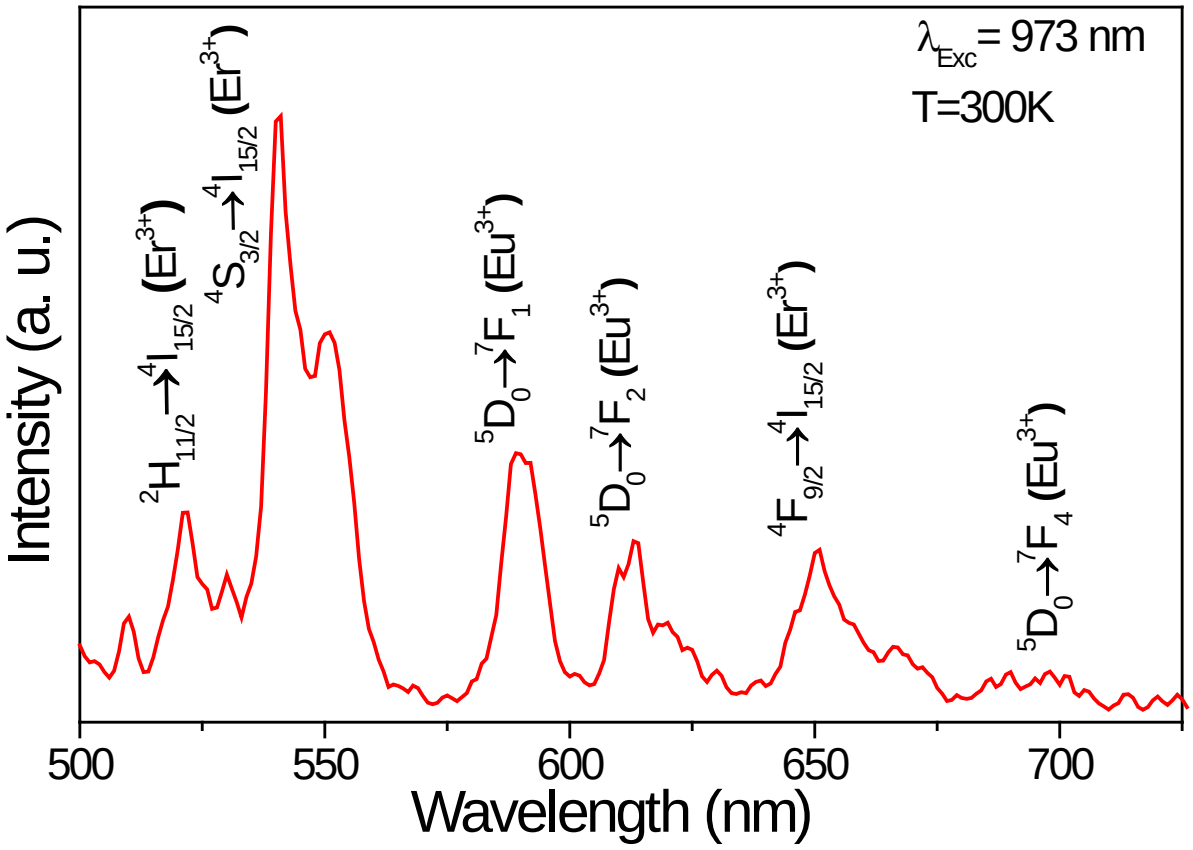

Fig. 7. Experimental emission decays (λ_{exc} = 380 nm, λ_{em} = 590 nm) of the $^5D_0$ level of Eu^{3+} in α-$NaYF_4$: x % Eu^{3+} (x =1, 5, 10, 20, 30). Solid lines represent fitting decays plotted using bi-exponential function (one in the rise and the other in the tail of the decays) for lower dopant concentration samples and using the I-H model for higher dopant concentration samples.

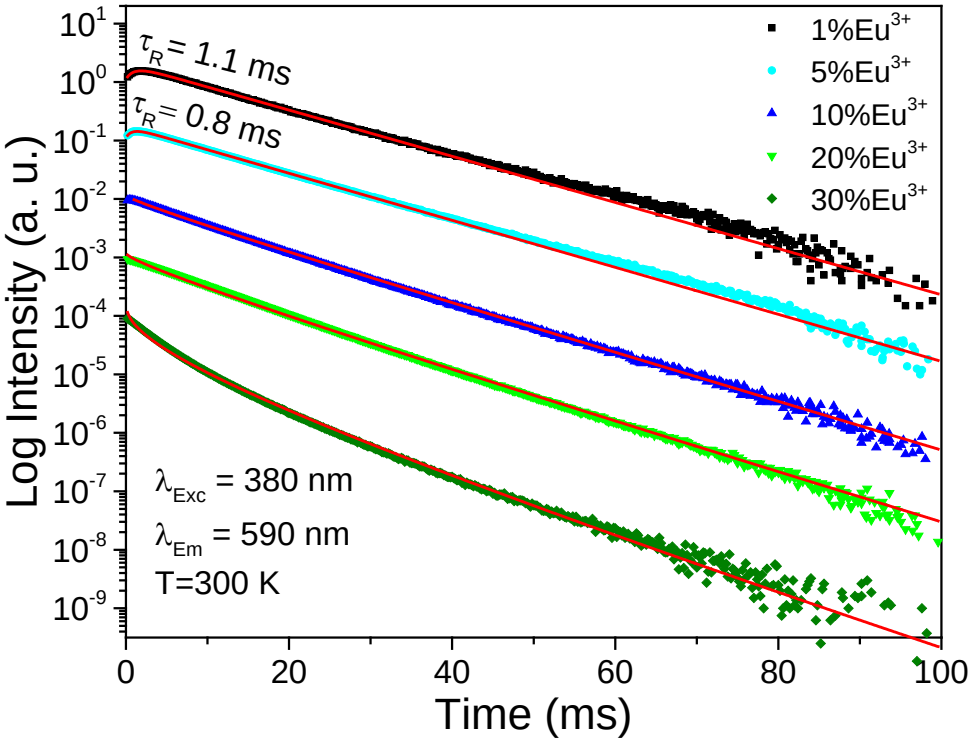

Fig. 8. Experimental emission decays (λ_{exc} = 380 nm, λ_{em} = 590 nm) of the $^5D_0$ level of Eu^{3+} in α-$NaYF_4$: 10 % Eu^{3+} / 20 % Yb^{3+} and of Eu^{3+} in α-$NaYF_4$: 10 % Eu^{3+} For comparison. Solid lines represent fitting decay derived using the I-H model.

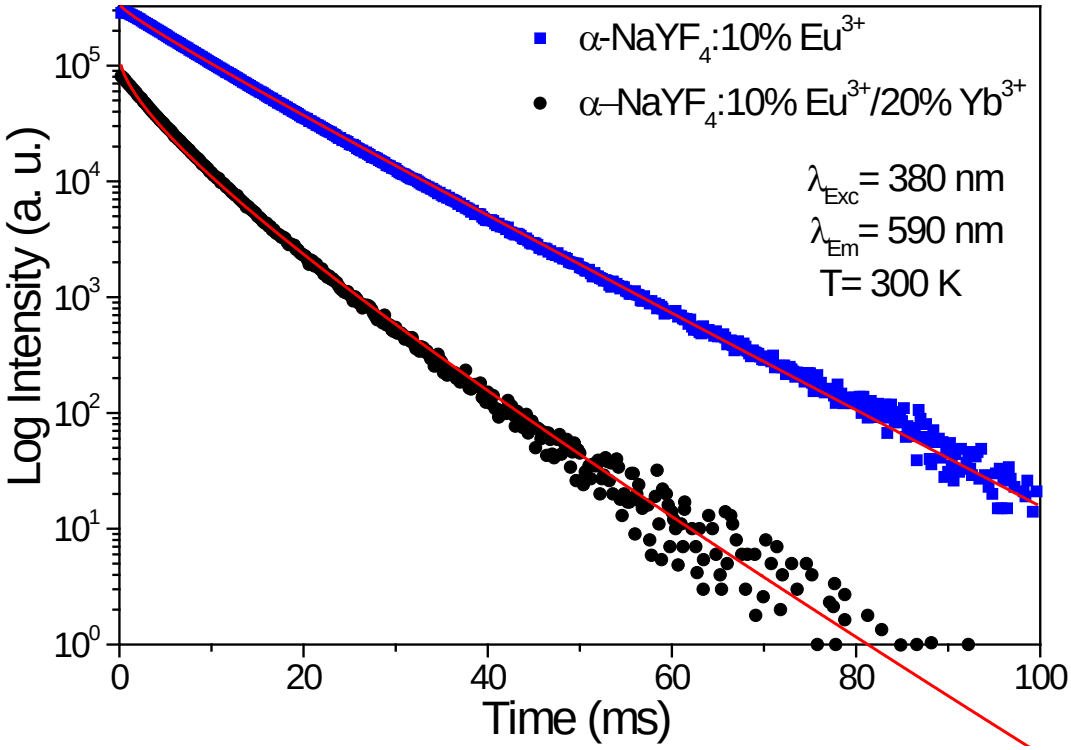

Fig. 9. Experimental up-converted emission decays of both Eu^{3+} : $^5D_0$ (λ_{em} = 590 nm) and Er^{3+} : $^4S_{3/2}$ (λ_{em} = 546 nm) excited levels in α-$NaYF_4$ doped 10 % Eu^{3+} / 20 % Yb^{3+} under laser excitation at 973 nm. Solid lines represent fitting decay derived using bi-exponential function.

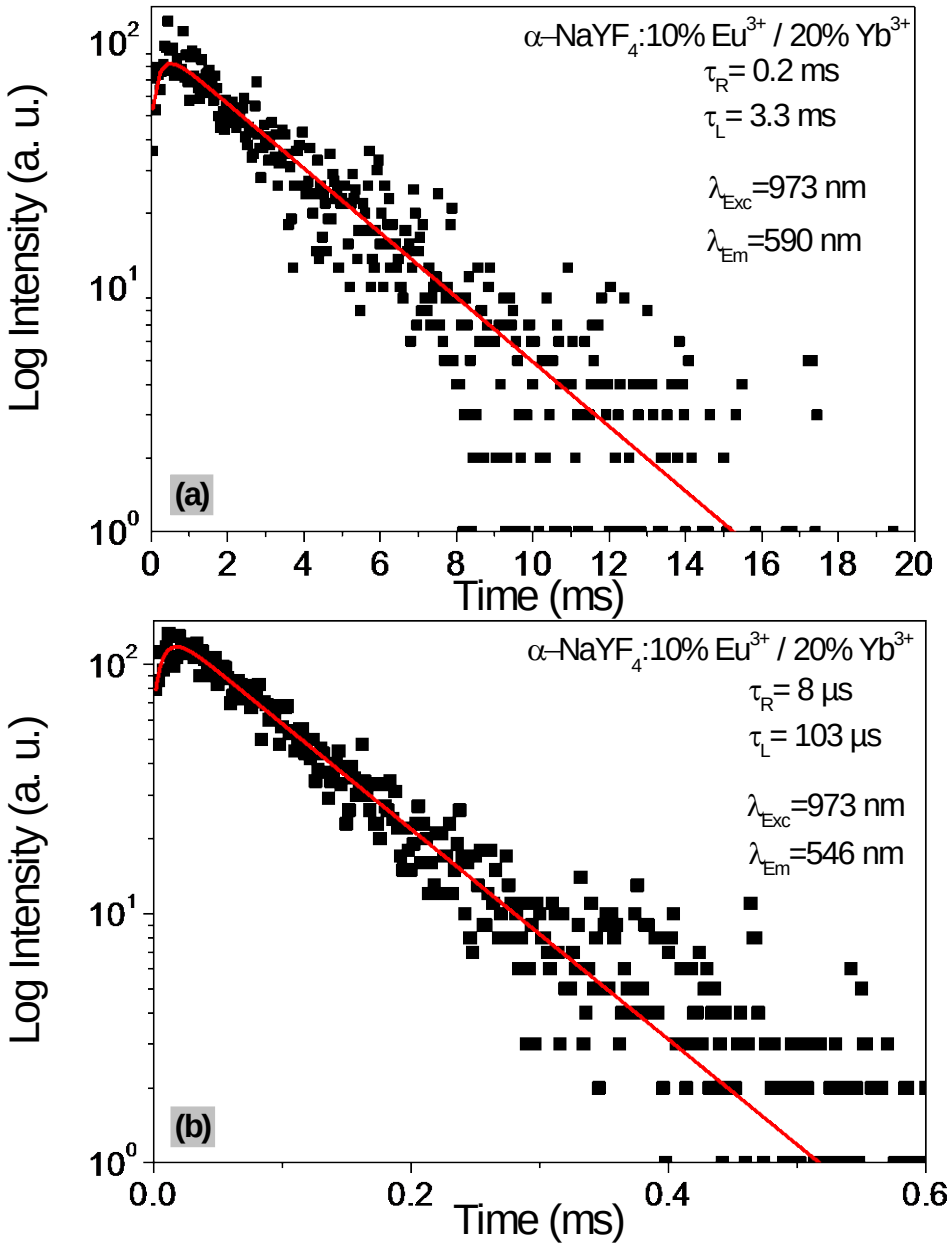

Fig. 10. Energy level diagram of the Eu^{3+} and Yb^{3+} ions as well as the proposed UC mechanism in α-$NaYF_4$: Eu^{3+}/Yb^{3+}.

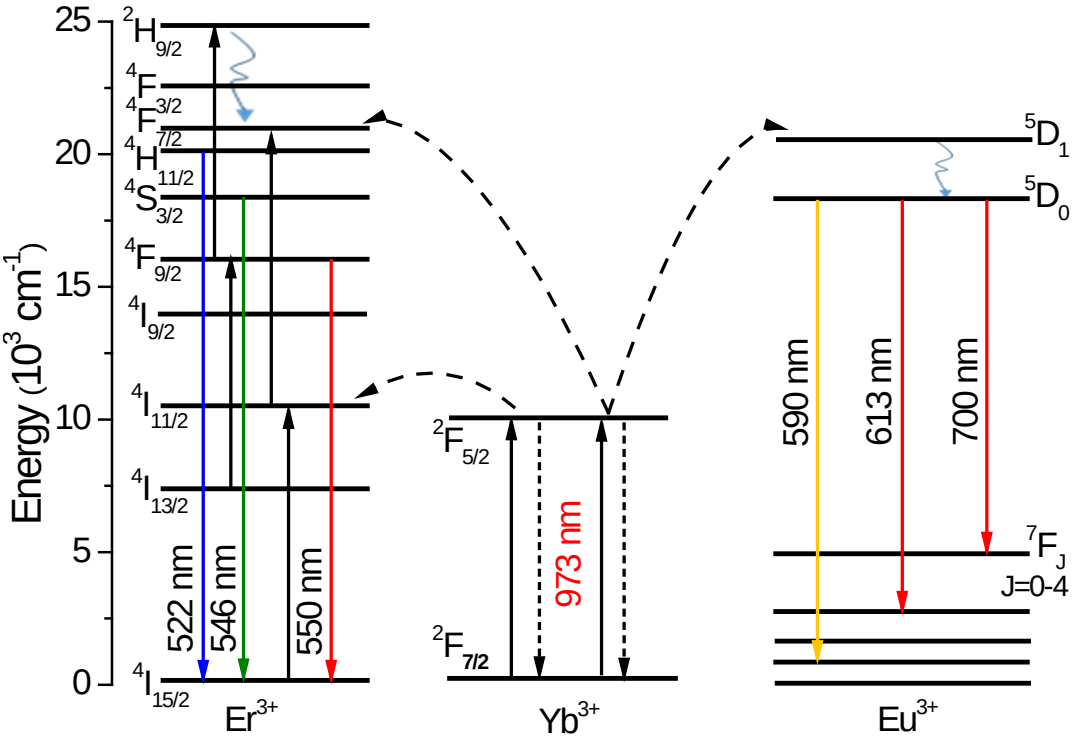

Fig. 11. Emission spectra of (1, 5, 10, 20, 30) % Tb^{3+} doped α-$NaYF_4$ under UV excitation at 380 nm. The inset shows the magnification of emission arising from the $^5D_3$ level of Tb^{3+}.

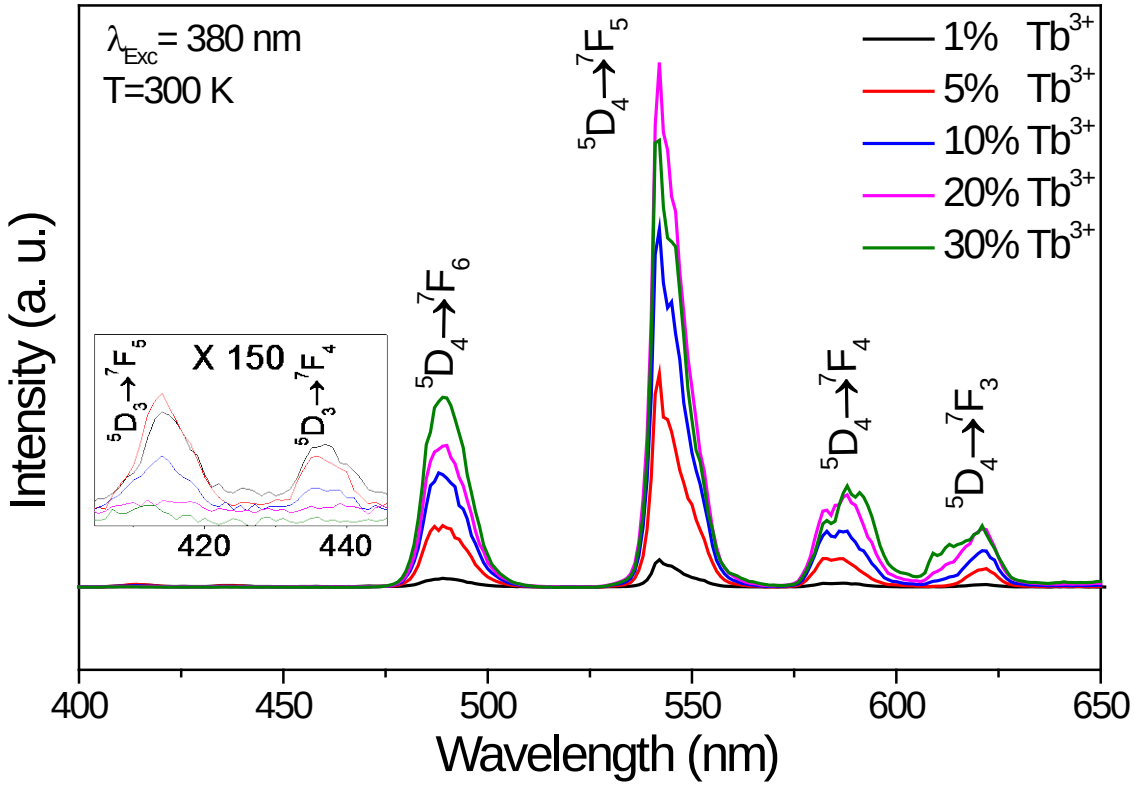

Fig. 12. Emission spectrum of 10%Tb^{3+}/20%Yb^{3+} co-doped α-$NaYF_4$ under excitation at 973nm.

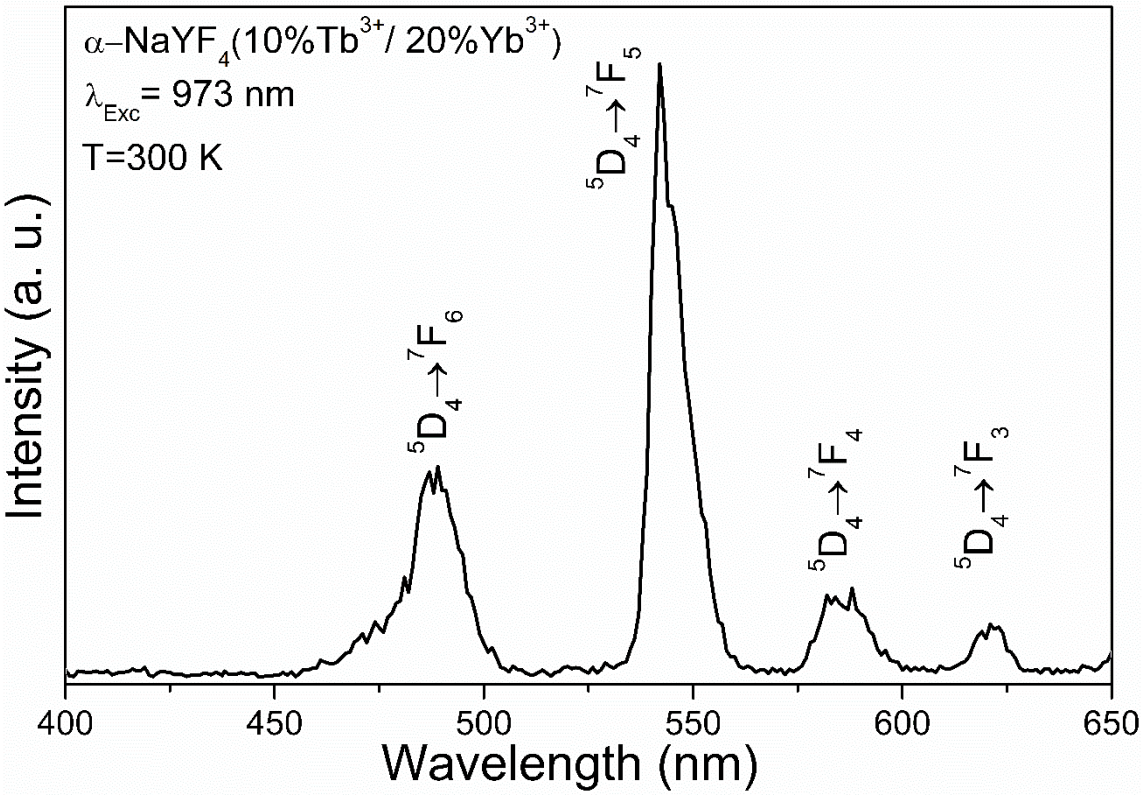

Fig. 13. Energy level diagram of Yb^{3+}/Tb^{3+} co-doped α-$NaYF_4$ as well as the proposed UC mechanism.

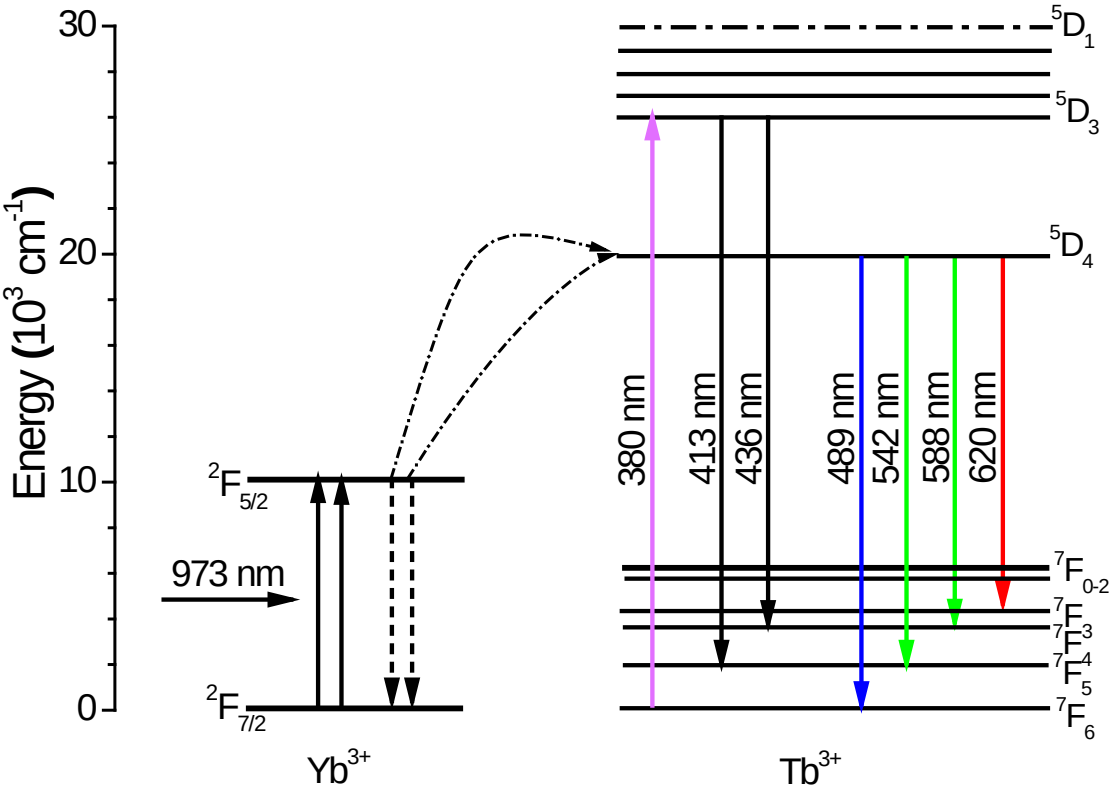

Fig. 14. Decay curves of the $^5D_4$ excited level of Tb^{3+} in α-$NaYF_4$ doped Tb^{3+} under UV excitation at 380 nm. Solid lines represent fitting decays derived using non-exponential function (one in the rise and other in the tail of the decays) for lower dopant concentration samples, and using the I-H model for 30 % dopant concentration sample.

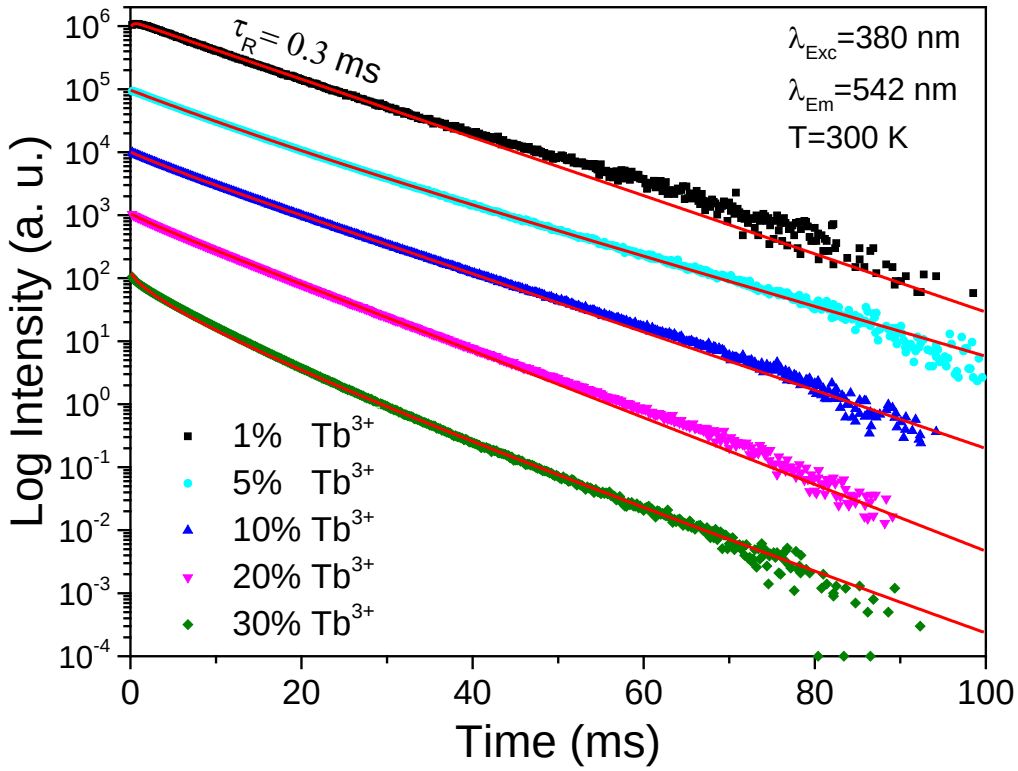

Fig. 15. Decay curves of the $^5D_4 \rightarrow {}^7F_5$ transition of Tb^{3+} in 10 % Tb^{3+} / 20 % Yb^{3+} co-doped α-$NaYF_4$ under IR and UV excitation. Solid lines represent fitting decay derived using exponential function for UV excitation, and using the I-H model for NIR excitation.

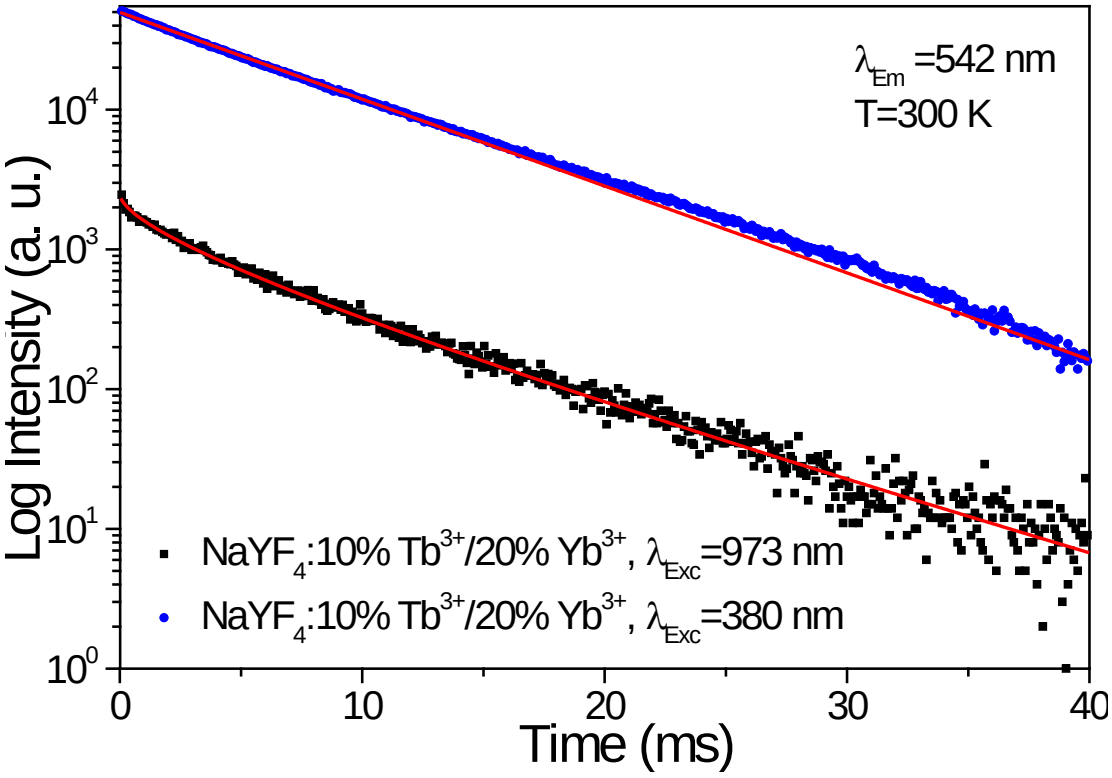

Table 1. Symmetry classes of the normal vibrations of ethylene glycol Vs frequencies.

Vibrations	Frequencies (cm^{-1})
OH stretching s	3330
CH stretching s	[2937-2878]
CH_2 scissoring	1450
OH bending and CH_2 wagging m	[1410-1315]
CH_2 twisting w	[1200-1254]
CO stretching vs	1094
CC stretching vs	1046
CH_2 rocking s	[887-866]
OH torsion vs	650

Table 2. Positional parameters and site occupation factors (SOF) of cubic α-$NaYF_4$ crystals.

Phase	**Atom**	**Site**	**x/a**	**y/b**	**z/c**	**SOF**
Cubic	Y	4a	0	0	0	0.5
(*Fm-3m*)	Na	4a	0	0	0	0.5
	F	8c	0.25	0.25	0.25	1

Table 3. The experimental values of C_A/C_0, critical concentration (C_0), energy transfer microparameter (C_{DA}), and critical distance (R_0) obtained from I-H model.

Sample	C_A/C_0	C_A (10^{20} ions/cm^3)	C_0 (10^{20} ions/cm^3)	C_{DA} (10^{-44} cm^6s^{-1})	R_0 (Å)
α-$NaYF_4$ [10% Eu^{3+}]	0.2	12.1	71	9.8	3.2
α-$NaYF_4$ [20% Eu^{3+}]	0.3	24	85	6.6	3
α-$NaYF_4$ [30% Eu^{3+}]	0.8	36	46	23.3	3.7

Table 4. The experimental values of C_A/C_0, critical concentration (C_0), energy transfer microparameter (C_{DA}), and critical distance (R_0) obtained from I-H model.

Sample	C_A/C_0	C_A (10^{20} ions/cm^3)	C_0 (10^{20} ions/cm^3)	C_{DA} (10^{-44}cm^{6}s^{-1})	R_0 (Å)
α-$NaYF_4$: [10% Eu^{3+}/20%Yb^{3+}]	0.9	36	40	32	3.9
α-$NaYF_4$: [10% Eu^{3+}/20%Yb^{3+}]	0.9	24	27	75.5	4.5

Table 5. Integrated intensity ratios in α-$NaYF_4$: 1% Eu^{3+} compounds (The notation In/I1 refers to the intensity ratios $^5D_0\rightarrow{}^7F_n/^5D_0\rightarrow{}^7F_1$ where n= (0, 2, 3, 4).

Item	Barycenter (cm^{-1})	Intensity Ratio
$^5D_0\rightarrow{}^7F_0$ (I0)	17301	
$^5D_0\rightarrow{}^7F_1$ (I1)	16891.9	I0/I1=0.01
$^5D_0\rightarrow{}^7F_2$ (I2)	16313.2	I2/I1=0.8 **(R)**
$^5D_0\rightarrow{}^7F_3$ (I3)	15384.6	I3/I1=0.03
$^5D_0\rightarrow{}^7F_4$ (I4)	14306.2	I4/I1=0.22

Table 6 . S_{ED}: The strength of an electrical dipole, S_{MD}: The strength of an magnetic dipole, A (J, J'): Probabilities of each spontaneous emission (radiative rates).

Transition	$\lambda_{(nm)}$	S_{ED} $10^{-65}C^2m^2$	S_{MD} $10^{-65}C^2m^2$	A(J,J') S^{-1}
$^5D_0\rightarrow{}^7F_1$	590		10.44	35.23
$^5D_0\rightarrow{}^7F_2$	613	9.83		26.32
$^5D_0\rightarrow{}^7F_4$	700	3.06		5.50

Table 7. Comparison of the J-O parameters for the $^5D_0 \rightarrow {}^7F_2$ (Ω_2) and $^5D_0 \rightarrow {}^7F_4$ (Ω_4) transitions of Eu^{3+} in similar materials.

	This work	[45]	[46]
$\Omega_2 \times 10^{-20} cm^2$	1.2	5.03	6.13
$\Omega_4 \times 10^{-20} cm^2$	0.52		5.88

Table 8. Calculated branching ratios of α-$NaYF_4$: 1%Eu^{3+}.

	β (0 →0)	β (0 →1)	β (0 →2)	β (0 →3)	β (0 →4)
α-$NaYF_4$: 1%Eu^{3+}	0.006	0.48	0.39	0.02	0.1

Table 9. The experimental values of C_A/C_0, critical concentration (C_0), energy transfer microparameter (C_{DA}), and critical distance (R_0) obtained from I-H model.

Sample	C_A/C_0	C_A (10^{20} ions/cm^3)	C_0 (10^{20} ions/cm^3)	C_{DA} ($10^{-44} cm^6 s^{-1}$)	R_0 (Å)
α-$NaYF_4$: [30%Tb^{3+}]	0.8	36	46	23.3	3.7

Table 10. The experimental values of C_A/C_0, critical concentration (C_0), energy transfer microparameter (C_{DA}), and critical distance (R_0) obtained from I-H model.

Sample	C_A/C_0	C_A (10^{20} ions/cm^3)	C_0 (10^{20} ions/cm^3)	C_{DA} ($10^{-44} cm^6 s^{-1}$)	R_0 (Å)
α-$NaYF_4$: [10%Tb^{3+}/20%Yb^{3+}]	0.7	36	54	16.7	3.5
α-$NaYF_4$: [10%Tb^{3+}/20%Yb^{3+}]	0.7	24	36	52.3	4.1